Environmental Science & Technology

Article

Cite This: Environ. Sci. Technol. 2019, 53, 14387−14397

pubs.acs.org/est

Methanesulfonic Acid-driven New Particle Formation Enhanced by Monoethanolamine: A Computational Study

Jiewen Shen,[†] Hong-Bin Xie,*[,†] Jonas Elm,[‡] Fangfang Ma,[†] Jingwen Chen,[†] and Hanna Vehkamäki[§]

[†]Key Laboratory of Industrial Ecology and Environmental Engineering (Ministry of Education), School of Environmental Science and Technology, Dalian University of Technology, Dalian 116024, China

[‡]Department of Chemistry and iClimate, Aarhus University, Langelandsgade 140, DK-8000 Aarhus C, Denmark

[§]Institute for Atmospheric and Earth System Research/Physics, University of Helsinki, P.O. Box 64, Gustaf Hällströmin katu 2a, FI-00014 Helsinki, Finland

Supporting Information

ABSTRACT: Amines are recognized as significant enhancing species on methanesulfonic acid (MSA)-driven new particle formation (NPF). Monoethanolamine (MEA) has been detected in the atmosphere, and its concentration could be significantly increased once MEA-based postcombustion CO_2 capture technology is widely implemented. Here, we evaluated the enhancing potential of MEA on MSA-driven NPF by examining the formation of MEA−MSA clusters using a combination of quantum chemical calculations and kinetics modeling. The results indicate that the −OH group of MEA can form at least one hydrogen bond with MSA or MEA in all MEA-containing clusters. The enhancing potential of MEA is higher than that of the strongest enhancing agent known so far, methylamine (MA), for MSA-driven NPF. Such high enhancing potential can be ascribed to not only the higher gas-phase basicity but also the role of the additional −OH group of MEA in increasing the binding free energy by forming additional hydrogen bonds. This clarifies the importance of hydrogen-bonding capacity from the nonamino group of amines in enhancing MSA-driven NPF. The main growth pathway for MEA−MSA clusters proceeds via the initial formation of the $(MEA)_1(MSA)_1$ cluster, followed by alternately adding one MSA and one MEA molecule, differing from the case of MA−MSA clusters.

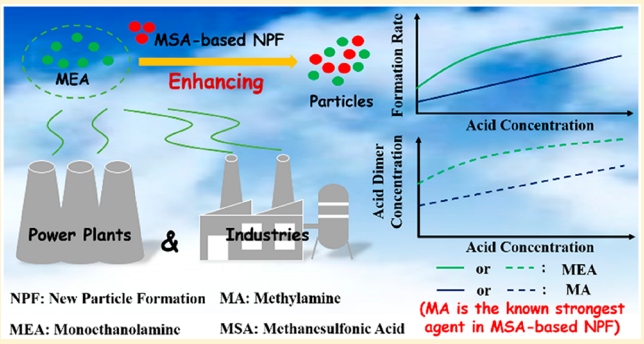

INTRODUCTION

New particle formation (NPF) represents the most important source of aerosol particles in the atmosphere.[1−4] Aerosol particles have a large influence on the global climate and human health.[3,5−9] A molecular-level understanding of NPF is crucial for assessing the impacts of aerosols and developing optimal control strategies.[10,11] There is compelling evidence that sulfuric acid (SA) is a key NPF precursor in many atmospheric environments.[3,4,12−21] Many studies have revealed that atmospheric bases (such as methylamine (MA), dimethylamine (DMA), trimethylamine (TMA), and ammonia) and organic acids (such as aromatic acids, dicarboxylic acids, and *cis*-pinonic acid) can efficiently enhance SA-driven NPF.[1,3,5,12,22−28] However, SA-driven NPF alone still cannot explain the observed NPF rates globally.[4,5,7,21,29−32] Therefore, in recent years, great efforts have been made to better understand NPF by considering the involvement of other gaseous species.

Besides SA, methanesulfonic acid (MSA) has been identified as an important NPF precursor.[29,33−36] MSA will play a more important role in NPF after the implementation of stricter regulations on SO_2 emission of fossil fuel combustion.[33,37] MSA is mainly derived from the oxidation of organosulfur compounds (OSCs) coming from oceans, agricultural activity, forest cover, and even human exhalation.[33,38] The atmospheric concentration of MSA is on the order of 10^5−10^7 molecules cm^{-3}, about 10%−100% of that of SA.[39,40] Since the binary nucleation efficiency of MSA−H_2O is extremely low under typical atmospheric conditions,[36] the contribution of MSA to NPF has been identified to highly depend on the enhancing effect of other species, primarily from atmospheric bases.[29,41] Therefore, identifying the atmospheric bases with strong enhancing potential on MSA-driven NPF is important to fully understand the contribution of MSA to NPF.

Currently, the studied atmospheric bases for MSA-driven NPF include MA, DMA, TMA, and ammonia, all of which have a significant enhancing effect.[29,41] MA was found to be

Received: September 3, 2019
Revised: November 4, 2019
Accepted: November 11, 2019
Published: November 11, 2019

DOI: 10.1021/acs.est.9b05306
Environ. Sci. Technol. 2019, 53, 14387−14397

the strongest species to enhance MSA-driven NPF,[41,42] in contrast to DMA which is the strongest one for SA-driven NPF.[2,12] Relative to DMA (one N−H bond site) and TMA (no N−H bond site), the higher enhancing potential of MA is ascribed to its higher hydrogen-bonding capacity from the amino group (two N−H bonds sites),[41] although its basicity is lower than that of DMA and TMA (gas-phase basicity (GB) for MA is 864.5 kJ mol^{-1}, for DMA 896.5 kJ mol^{-1}, and for TMA 918.1 kJ mol^{-1}).[43] Relative to ammonia, it is ascribed to the higher basicity of MA (GB for ammonia is 819.0 kJ mol^{-1}).[41,43] This implies that both basicity and hydrogen-bonding capacity contribute to the enhancing potential of an atmospheric base on MSA-driven NPF.[11,41,44,45] Therefore, atmospheric bases with stronger gas-phase basicity and higher hydrogen-bonding capacity than MA could be even more efficient enhancing agents for MSA-driven NPF.

Monoethanolamine (MEA) is a benchmark and widely utilized solvent in amine-based postcombustion CO_2 capture (PCCC) technology and feed stock for the chemical and pharmaceutical industries.[46−52] Previous studies have shown that a CO_2 capture plant of MEA-based PCCC could potentially emit 80 tons MEA into the atmosphere for each 1 million tons of CO_2 removed per year.[53,54] Thus, once MEA-based PCCC technology has been implemented on a large-scale, it is likely that there will be significant discharges of MEA to the atmosphere from PCCC units.[11,55] Even though PCCC technology is not yet used on a large scale, current global production of ethanolamines (including MEA, diethanolamine, and triethanolamine) could be surprisingly high. For instance, production of ethanolamines in America can reach up to 3×10^5 ton per year.[52] MEA has been detected as a significant component of $PM_{2.5}$ in various locations.[56−58] In recent field measurements, it was found that MEA is one of the two most abundant amines in $PM_{2.5}$ in Shanghai.[56] Compared to MA, MEA has higher GB (896.8 kJ mol^{-1})[43] and higher hydrogen-bonding capacity due to its additional −OH group.[11] Therefore, MEA could have a higher enhancing potential on MSA-driven NPF than MA. However, to the best of our knowledge, no previous study has addressed the participation of MEA in MSA-driven NPF and the role of additional hydrogen-bonding capacity from the nonamino group in enhancing MSA-driven NPF.

Using quantum chemical methods and the Atmospheric Cluster Dynamics Code (ACDC),[59] we investigated the participation of MEA in the initial steps in MSA-driven NPF by examining the cluster formation between MEA and MSA. We have obtained the minimum free energy structures of the $(MEA)_m(MSA)_n$ (m = 0−4, n = 0−4) clusters and use the calculated thermodynamic data as input for ACDC simulations to obtain cluster formation pathways and rates. In addition, the effect of hydration on cluster formation kinetics was also considered.

COMPUTATIONAL DETAILS

Electronic Structure Calculations. The global minimum structures of the pure $(MEA)_{1-4}$ clusters were taken from our previous study.[11] A multistep global minimum sampling scheme, which has been applied to study atmospheric cluster formation in previous studies,[11,60−63] was employed to search for the global minima of the $(MEA)_m(MSA)_n$ (m = 0−4, n = 1−4) clusters. The details for the scheme were presented in our previous study.[11,63] Briefly, around 10,000 initial random configurations for each cluster were gradually screened, using various theoretical methods, to find the configuration with the lowest free energy. The employed theoretical methods include PM6, ωB97X-D/6-31+G(d,p), ωB97X-D/6-31++G(d,p), and DLPNO−CCSD(T)/aug-cc-pVTZ. The ωB97X-D/6-31++G-(d,p) level of theory was applied for optimization of geometries and calculation of vibrational frequencies, and the DLPNO-CCSD(T)/aug-cc-pVTZ level of theory was used for calculating the single point energy. Geometry optimization, frequency, or single point energy calculations at the PM6 and ωB97X-D level of theory were performed in the GAUSSIAN 09 program package.[64] DLPNO-CCSD(T)/aug-cc-pVTZ calculations were performed using the ORCA 4.0.0 program package with tight SCF and PNO convergence criteria.[65] The ωB97X-D/6-31++G(d,p) level and DLPNO-CCSD(T)/aug-cc-pVTZ level of theory were selected as the core optimization/frequency and single point energy calculation method, respectively, since they have shown good performance for studying the formation of atmospheric molecular clusters.[66−70] The Gibbs free energy for each global minima was calculated at 298.15 K by combining the single point energies at the DLPNO-CCSD(T)/aug-cc-pVTZ level and the Gibbs free energy correction terms at the ωB97X-D/6-31++G(d,p) level. The cluster formation free energy (ΔG) was obtained by subtracting the Gibbs free energy of the constituent molecules from that of the cluster at 298.15 K. The formation free energies at other temperatures were calculated by assuming that enthalpy and entropy change remain constant in the considered tropospheric temperature range.

To probe the effect of hydration, the $(MEA)_m(MSA)_n(H_2O)_x$ (m = 0−2, n = 0−2, x = 1−3) clusters were investigated. The global minima of $(MEA)_{1-2}(H_2O)_{1-3}$ were taken from our previous study.[11] The same scheme as for unhydrated $(MEA)_m(MSA)_n$ clusters was used to locate the global minima of the $(MEA)_m(MSA)_n(H_2O)_x$ (m = 0−2, n = 1−2, x = 1−3) clusters. In addition, to compare the enhancing potential of MEA with MA, the cluster formation free energies for $(MA)_{0-2}(MSA)_{0-2}$ were calculated at the same level of theory as for the $(MEA)_m(MSA)_n$ clusters. The $(MA)_1(MSA)_1$, $(MA)_2(MSA)_2$, and $(MA)_1(MSA)_2$ cluster structures are available in the literature,[41,71] and the structures of the $(MA)_2$ and $(MA)_2(MSA)_1$ clusters were obtained in this work. It deserves mentioning that there are two reported global minima for cluster $(MA)_1(MSA)_1$.[71,72] One involves proton transfer between MA and MSA, and the other does not. The one without the proton transfer, which was determined to have lower free energy at the theoretical level of this work, was selected.

ACDC Simulation. ACDC was employed to investigate the cluster steady-state (i.e., time independent) concentration, formation pathways, and formation rates of MEA−MSA clusters.[59] In ACDC, the birth−death equation (eq 1) is used to describe the time (t) evolution of molecular cluster distributions

$$\frac{dc_i}{dt} = \frac{1}{2}\sum_{j<i}\beta_{j,(i-j)}c_j c_{(i-j)} + \sum_j \gamma_{(i+j)\to i}c_{i+j} - \sum_j \beta_{i,j}c_i c_j - \frac{1}{2}\sum_{j<i}\gamma_{i\to j}c_i + Q_i - S_i \quad (1)$$

DOI: 10.1021/acs.est.9b05306
Environ. Sci. Technol. 2019, 53, 14387−14397

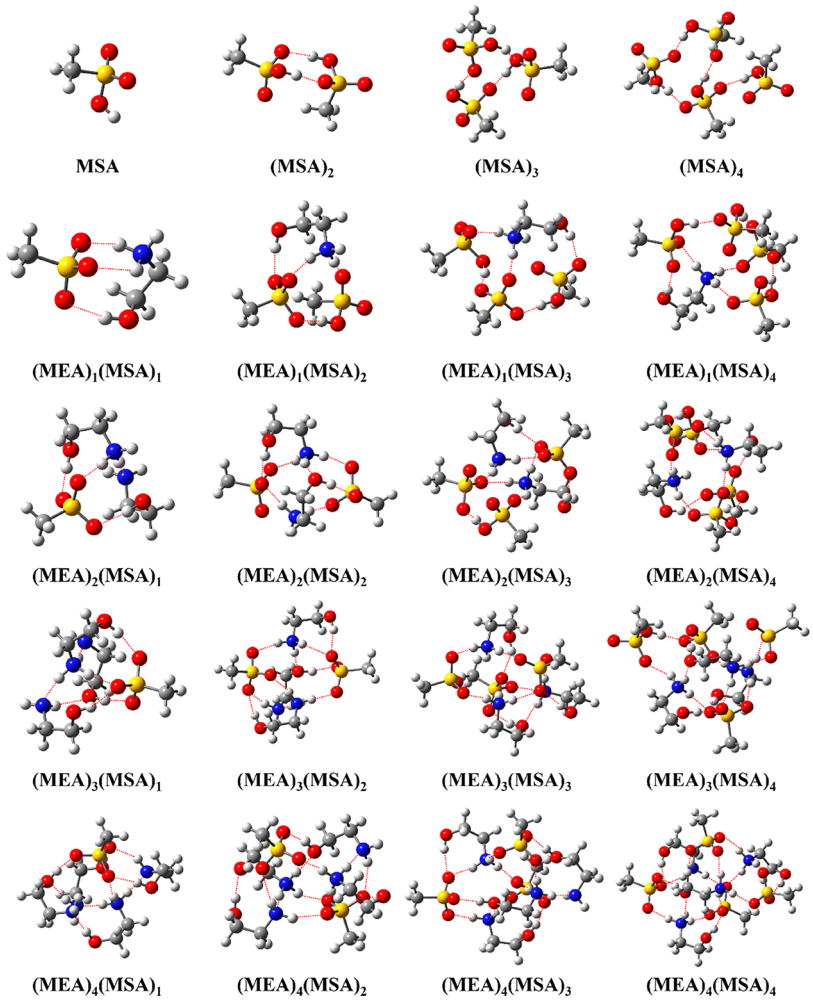

Figure 1. Lowest Gibbs free energy conformations of the $(MEA)_m(MSA)_n$ (m = 0−4, n = 1−4) clusters at the DLPNO-CCSD(T)/aug-cc-pVTZ//ωB97X-D/6-31++G(d,p) level of theory. Red balls represent oxygen atoms, blue for nitrogen atoms, gray for carbon atoms, and white for hydrogen atoms. Dashed red lines indicate hydrogen bonds.

where subscripts i, j, $i-j$, $j-i$, and $i+j$ represent different clusters (or monomers) in the system, c represents the concentration of a cluster (or monomer), β is the collision coefficient between two clusters (or monomers), γ represents the evaporation coefficient of a cluster ($i + j$) which evaporates into its daughter cluster (i) as illustrated by the arrow of the subscript. Q_i represents additional outside sources, and S_i represents the sink terms. β and γ were calculated by eq 2 and eq 3 (taking $\beta_{i,j}$ and $\gamma_{(i+j)\rightarrow i}$ as examples), respectively.

$$\beta_{i,j} = \left(\frac{3}{4\pi}\right)^{1/6}\left(\frac{6k_bT}{m_i} + \frac{6k_bT}{m_j}\right)^{1/2}(V_i^{1/3} + V_j^{1/3})^2 \quad (2)$$

where k_b represents the Boltzmann constant, T represents the temperature, and m and V are the mass and volume of the cluster (or monomer), respectively.

$$\gamma_{(i+j)\rightarrow i} = \beta_{i,j}c_{\mathrm{ref}}\exp\left\{\frac{\Delta G_{i+j} - \Delta G_i - \Delta G_j}{k_bT}\right\} \quad (3)$$

where ΔG represents the formation free energy of a cluster, c_{ref} is the reference monomer concentration at 1 atm, which is the pressure at which ΔG was calculated.

Here, the ACDC simulation system was treated as a "4 × 4 box" for the unhydrated MEA−MSA cluster system, where 4 is the maximum number of MEA or MSA molecules in the cluster. The $(MEA)_4(MSA)_5$ and $(MEA)_5(MSA)_5$ clusters were set as the boundary clusters that are allowed to leave the simulation and contribute to NPF (see detailed description in the Supporting Information (SI)). In the simulation, the MSA concentration [MSA] was set to be 10^5, 10^6, 10^7, and 10^8 molecules cm^{-3} and the MEA concentration [MEA] to 1 ppt (~2.50×10^7 molecules cm^{-3}), 10 ppt (~2.50×10^8 molecules cm^{-3}), and 100 ppt (~2.50×10^9 molecules cm^{-3}). The simulations were mainly run at 278.15 K, with additional runs at 258.15, 268.15, 278.15, 288.15, and 298.15 K, to probe the effect of temperature. Since there is no available value of the coagulation sink coefficient for MSA vapor, we chose a constant coagulation sink coefficient of 2.60×10^{-3} s^{-1} to account for the loss of clusters. This value is based on the median condensation sink of sulfuric acid vapor on pre-existing aerosol particles at Hyytiälä, Finland.[73,74] In addition, within the range from 6×10^{-4} to 6×10^{-2} s^{-1}, covering possible condensation sink coefficients in clean and haze days,[75,76] the effect of coagulation sink coefficient on results is examined. One was used as the sticking factor in all simulations with additional tests at 0.1 and 0.01.[59,73] Unless noted, 2.60×10^{-3} s^{-1} for the coagulation sink coefficient, 1 for the sticking factor, and 278.15 K for the temperature are used throughout ACDC

DOI: 10.1021/acs.est.9b05306
Environ. Sci. Technol. 2019, 53, 14387−14397

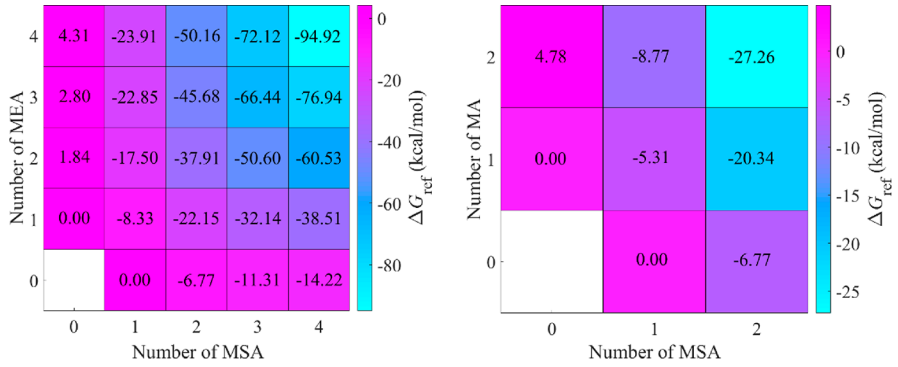

Figure 2. Gibbs free binding energy of the $(MEA)_m(MSA)_n$ (m = 0−4, n = 0−4) clusters (left panel) and $(MA)_a(MSA)_b$ (a = 0−2, b = 0−2) clusters (right panel) calculated at the DLPNO-CCSD(T)/aug-cc-pVTZ//ωB97X-D/6-31++G(d,p) level of theory. The calculations are performed at 298.15 K and 1 atm.

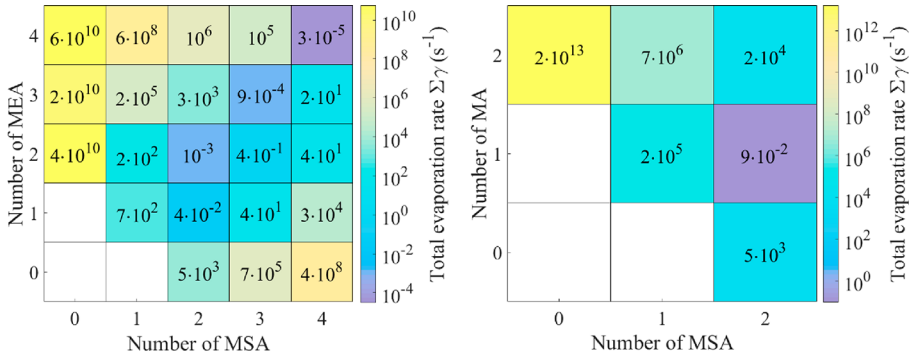

Figure 3. Evaporation rates of $(MEA)_m(MSA)_n$ (m = 0−4 and n = 0−4) (left panel) and $(MA)_a(MSA)_b$ clusters (a = 0−2 and b = 0−2) (right panel) at 278.15 K.

simulation. For the hydrated MEA−MSA cluster, the simulation system was treated as a "2 × 2 box", and the clusters $(MEA)_2(MSA)_3$ and $(MEA)_3(MSA)_3$ were set as the boundary clusters. The simulation was run at 278.15 K with [MEA] = 10 ppt (~2.50×10^8 molecules cm^{-3}) and [MSA] = 10^6 molecules cm^{-3}.

An ACDC simulation was also performed using a "2 × 2 box" for the MA−MSA system as a comparison. $(MA)_2(MSA)_3$ and $(MA)_3(MSA)_3$ were set as the boundary clusters, and other simulation settings were similar to those of the MEA−MSA system. In addition, we also run ACDC simulations for the MEA−MSA system with a "2 × 2 box" for a direct comparison with the MA−MSA system under the same conditions.

RESULTS AND DISCUSSION

Cluster Structures. The located lowest free energy conformations of the $(MEA)_m(MSA)_n$ (m = 0−4, n = 1−4) clusters are presented in Figure 1. All the identified cluster structures and thermochemistry have been added to the Atmospheric Cluster Database.[77] Here, we only discuss the $(MEA)_m(MSA)_n$ (m = 0−4, n = 1−4) clusters, since the pure $(MEA)_m$ (m = 1−4) clusters have been analyzed in our previous study.[11] In view of the molecular structure, the MSA molecule only has a single transferable proton (S−OH group), and the MEA molecule only has one available site ($-NH_2$ group) that can be protonated. Therefore, only a "one to one" proton transfer pattern can occur between MEA and MSA. As can be seen in Figure 1, there is no proton transfer in the homomolecular $(MSA)_n$ (n = 1−4) clusters, and the pure $(MSA)_n$ clusters are mainly stabilized by hydrogen bonds (H-bonds), similar to the case of $(MEA)_m$ (m = 1−4) clusters.[11] However, proton transfers occur in all the heteromolecular $(MEA)_m(MSA)_n$ (m = 1−4, n = 1−4) clusters, and the clusters are stabilized by both H-bonds and electrostatic interactions between positive and negative species. When MEA molecules are not less than MSA molecules in the clusters ($m \geq n$), all the MSA molecules donate their protons to the MEA molecules, and ($m - n$) MEA molecules remains unprotonated. In the case when there is an equal amount of acids and bases in the cluster ($m = n$), all MEA molecules are protonated. When there are more MSA molecules in the cluster compared to MEA ($m < n$), m of the MSA molecules donate their protons to m MEA molecules and ($n - m$) MSA molecules are kept intact. Thus, the number of proton transfers is equal to the lower value of m or n. In the case of all heteromolecular $(MEA)_m(MSA)_n$ (m = 1−4, n = 1−4) clusters where $m = n$, the number of proton transfers is equal to m or n.

Another structural feature observed in all heteromolecular $(MEA)_m(MSA)_n$ (m = 1−4, n = 1−4) clusters is that the −OH group in all MEA molecules can form at least one H-bond with MSA as a H-bond donor. In many of the clusters such as $(MEA)_2(MSA)_2$, $(MEA)_3(MSA)_1$, $(MEA)_3(MSA)_2$, $(MEA)_3(MSA)_3$, $(MEA)_3(MSA)_4$, $(MEA)_4(MSA)_1$, $(MEA)_4(MSA)_2$, $(MEA)_4(MSA)_3$, and $(MEA)_4(MSA)_4$, the −OH group of MEA can act as a H-bond acceptor and form additional H-bonds with the $-NH_2$ groups of MEAs, $-NH_3^+$ groups of protonated MEAs, or −OH group of another MEA. The participation of the −OH group of MEA in forming H-bonds was also found in the MEA−SA clusters in our previous study.[11] In addition, all protonated and unprotonated $-NH_2$ groups of MEA at least participate in one H-bond formation.

DOI: 10.1021/acs.est.9b05306
Environ. Sci. Technol. 2019, 53, 14387−14397

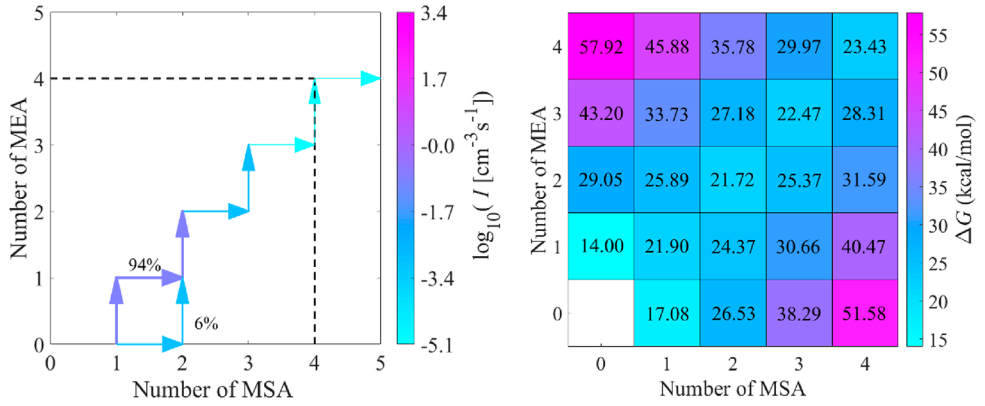

Figure 4. Cluster formation pathways (left panel) and actual formation free energy surface (right panel) for the MEA−MSA system at 278.15 K, [MSA] = 10^6 molecules cm^{-3}, and [MEA] = 10 ppt. For clarity, pathways contributing less than 5% to the flux of the cluster are not shown.

Such multiple H-bonds formed by MEA lead to the formation of an internal network in the MEA-containing clusters, which make the cluster prefer to form a spherical three-dimensional structure, especially for large MEA−MSA clusters. Actually, the formation of an internal H-bond network forces the hydrophobic $-CH_3$ group of MSA to be kept at the outer edge of the clusters.

Cluster Formation Free Energy Surface. MA is known as the strongest enhancing agent in MSA-driven NPF.[41,42] Here, ΔG values of the MA−MSA system were used as a comparison point for the MEA−MSA system. The formation free energy surface at 298.15 K for the MEA−MSA system is presented in Figure 2, along with that for the MA−MSA system (only the $(MA)_{0-2}(MSA)_{0-2}$ clusters are available). The corresponding thermodynamical quantities ΔH and ΔS are presented in Table S1. As can be seen in Figure 2, the ΔG value of each MEA-containing cluster is significantly lower than that of the corresponding MA-containing cluster within the available MA−MSA cluster size. The difference in ΔG values between the MEA−MSA cluster and the corresponding MA−MSA cluster is in the range of 1.81−10.65 kcal mol^{-1}. Combined with the cluster structure analysis in the previous section, we can conclude that such a large difference should result from both a higher gas-phase basicity and higher H-bonding capacity of MEA compared to those of MA.

Evaporation Rates. The evaporation rates of the clusters in the MEA−MSA system and the MA−MSA system are presented in Figure 3. As can be seen in Figure 3, the evaporation rates for the MEA−MSA clusters ($(MEA)_2(MSA)_2$, $(MEA)_3(MSA)_3$, and $(MEA)_4(MSA)_4$) along the diagonal line of the grid are much lower than those of the other clusters, with a range from 10^{-5} to 10^{-3} s^{-1}. Clusters with such low evaporation rates can be deemed stable against evaporation at atmospheric conditions when the concentration of MSA or MEA is at the ppt level (SI). In addition, the evaporation rates of the clusters above the diagonal line are much higher than those of the corresponding clusters beneath the diagonal line, indicating that MSA-abundant clusters are more stable than corresponding MEA-abundant clusters. By inspecting all possible evaporation pathways (SI), it was found that the evaporation of a MEA or MSA monomer is the main decay route for all clusters except $(MSA)_4$, for which the evaporation into two MSA dimers is the most favorable path. When $m \geq n$, the $(MEA)_m(MSA)_n$ clusters decay mainly via evaporation of a MEA monomer. Vice versa is observed for $m < n$, where the evaporation of a MSA monomer is dominant. For the largest studied $(MEA)_4(MSA)_4$ cluster, the rate for the evaporation route $(MEA)_4(MSA)_4 \rightarrow (MEA)_2(MSA)_2 + (MEA)_2(MSA)_2$ is close to that of the most favorable route $(MEA)_4(MSA)_4 \rightarrow (MEA)_3(MSA)_4 + MEA$, implying that the $(MEA)_2(MSA)_2$ cluster is relatively stable in the studied system.

We also compare the evaporation rates of MEA−MSA clusters with the corresponding MA−MSA clusters up to a 2 × 2 size of the MA−MSA clusters. As can be seen in Figure 3, the evaporation rate of each of the MA-containing clusters is in all cases higher than that of corresponding MEA-containing cluster. Therefore, we can conclude that MEA can form more stable clusters with MSA than MA at the same acid and base concentration.

Clusters Growth Pathways. Figure 4 shows the cluster growth pathways and actual Gibbs free energy surface for the MEA−MSA clusters at 278.15 K, [MSA] = 10^6 molecules cm^{-3}, and [MEA] = 10 ppt (~2.50 × 10^8 molecules cm^{-3}). As can be seen in Figure 4, the main pathway for MEA−MSA cluster growth is the following: the first step is the binding of one MSA molecule to one MEA molecule to form the $(MEA)_1(MSA)_1$ cluster. After the initial step, the growth mainly proceeds by first adding one MSA molecule and then one MEA molecule, similar to the case of the MEA−SA system.[11] In contrast to the MEA−SA system,[11] the $(MSA)_2$ acid dimer shows a nonnegligible contribution to the initially formed clusters. This could mainly result from the lower stability of the $(MEA)_1(MSA)_1$ cluster compared to that of $(MEA)_1(SA)_1$. Among the clusters fluxing out of the "4 × 4 box", $(MEA)_4(MSA)_5$ is the most prominent one with a 99% contribution. Comparing the growth pathway with the evaporation rate of the clusters, we can conclude that the formation of the initial $(MEA)_1(MSA)_1$ cluster is the rate-determining step for the cluster growth since the $(MEA)_1(MSA)_1$ cluster is the most unstable among all the clusters in the main cluster growth pathway. In addition, as shown in Figures S4 and S5, both the coagulation sink coefficient and sticking factor slightly affect the cluster growth pathways.

The cluster growth pathway of MEA−MSA clusters was compared with that of the corresponding MA−MSA clusters within the "2 × 2 box" size at the same simulation conditions (Figure S7). The significant difference in the cluster growth pathway between the two systems lies in the formation of the initial cluster. For the MEA−MSA system, the formed initial cluster is mainly $(MEA)_1(MSA)_1$; however, for the MA−MSA

DOI: 10.1021/acs.est.9b05306
Environ. Sci. Technol. 2019, 53, 14387−14397

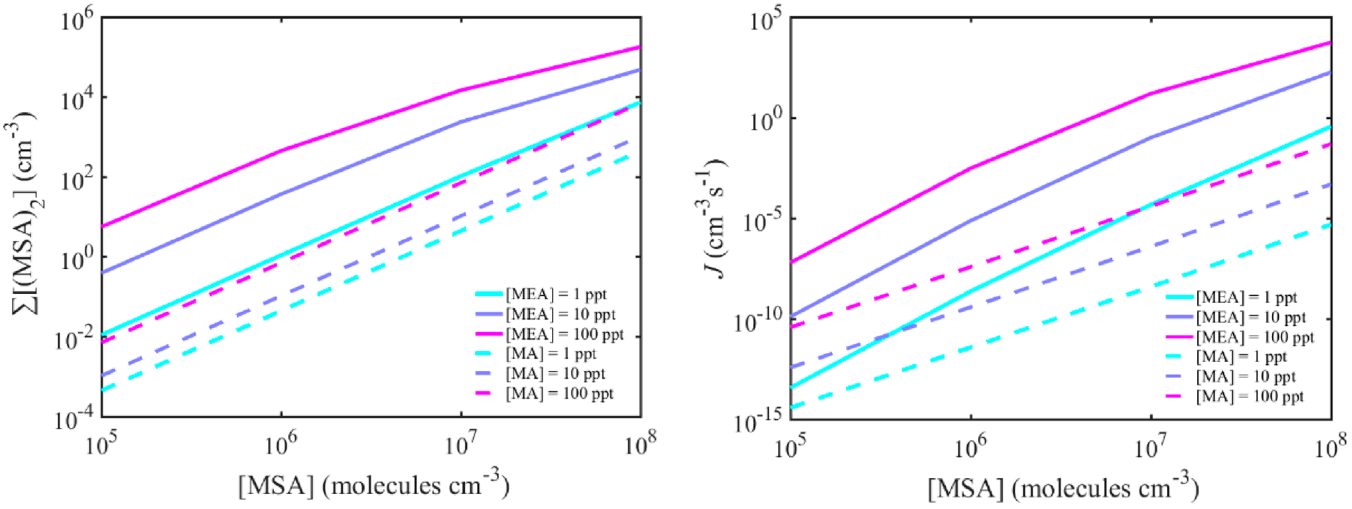

Figure 5. Simulated steady-state MSA dimer concentration $\Sigma[(MSA)_2]$ (cm^{-3}) and cluster formation rate J (cm^{-3} s^{-1}) as a function of monomer concentration at 278.15 K.

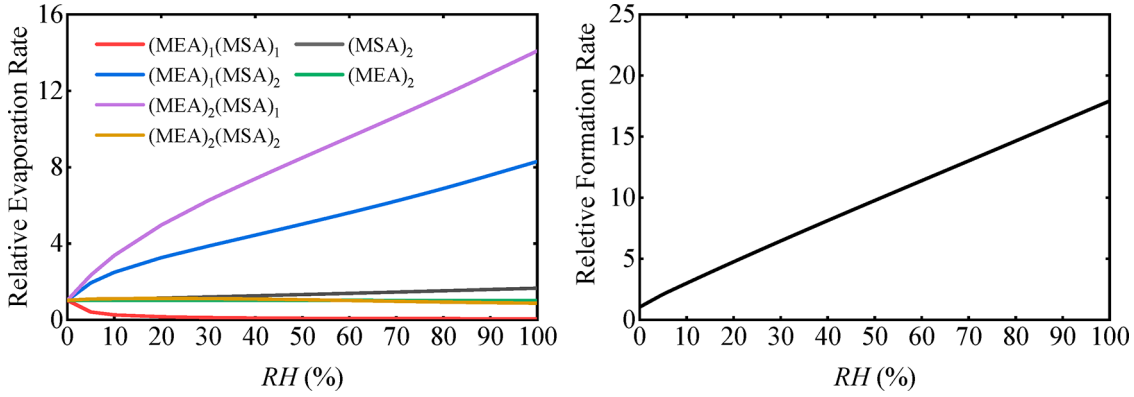

Figure 6. Relative evaporation rate (left panel) and cluster formation rate ([MSA] = 10^6 molecules cm^{-3} and [MEA] = 10 ppt) (right panel) as a function of relative humidity (RH) at 278.15 K.

system, the dominant initial cluster is the $(MSA)_2$ cluster. Such a difference can be explained by the higher stability of $(MEA)_1(MSA)_1$ compared to $(MA)_1(MSA)_1$ at the studied acid and base concentrations.

Steady-State Concentrations of MSA Dimer and Cluster Formation Rates. The steady-state concentration of the acid dimer ($\Sigma(MSA)_2$, all clusters including acid dimers) and cluster formation rate can be used to evaluate the enhancing potential of a given base on MSA-driven NPF similar to the case of SA-driven NPF.[11,25,78] Figure 5 presents the steady-state $\Sigma(MSA)_2$ concentration and cluster formation rate as a function of the concentration of MSA (10^5–10^8 molecules cm^{-3}) and MEA (1–100 ppt) for the MEA-MSA system at 278.15 K. The MA–MSA cluster system is included as a comparison. Figure 5 shows that with increasing concentration of MSA and MEA the $\Sigma(MSA)_2$ concentration and cluster formation rate gradually increase at the considered conditions. However, the effect of MEA concentration on the $\Sigma(MSA)_2$ concentration and cluster formation rate gradually become weaker with increasing MEA concentration. This is consistent over the entire considered MSA concentration range, especially in the case of high concentration of MSA. Therefore, the MEA–MSA system approaches saturation with respect to MEA. This behavior is not observed in the MA–MSA system. More importantly, both the $\Sigma(MSA)_2$ concentration and cluster formation rate for the MEA–MSA system are generally much higher than those of a corresponding MA–MSA system in the same concentration of MSA and base. For instance, MEA yields a 10–10^2-fold increase in $\Sigma(MSA)_2$ concentration and 10–10^5-fold increase in cluster formation rate compared to MA at the considered conditions. Another way of viewing this is that 0.44–0.63 ppt MEA ([MSA] = 10^6 molecules cm^{-3}) and 0.20–0.29 ppt MEA ([MSA] = 10^7 molecules cm^{-3}) can reach a similar enhancing effect as a MA concentration of 5–10 ppt (The equivalent concentration of MEA to MA was simply obtained by adjusting the concentration of MEA in ACDC simulations until the calculated cluster formation rate of MEA is similar to that of 5–10 ppt MA). Note that we compare a "4 × 4 box" simulation for the MEA–MSA system to the "2 × 2 box" simulation for the MA–MSA system. If a "2 × 2 box" size is used also for the MEA–MSA system, the difference in cluster formation rate becomes even more pronounced (SI). All in all, we can conclude that MEA has a significantly higher enhancing potential than MA on MSA-driven NPF.

Effect of Hydration. Hydration can affect the NPF kinetics and thermodynamics of MSA and bases.[79–81] Previous studies have shown that SA–base (base = ammonia, DMA, and MEA) clusters are mainly hydrated by less than three H_2O molecules.[13] Compared with SA, MSA is less hygroscopic

DOI: 10.1021/acs.est.9b05306
Environ. Sci. Technol. 2019, 53, 14387–14397

and thus should be less hydrated.[29] Here, one to three H_2O molecules were considered to study the effect of hydration on the formation kinetics of the MEA−MSA clusters. Similar to our previous studies,[11,63] only the smaller $(MEA)_m(MSA)_n$ (m = 0−2, n = 0−2) clusters were considered as a test to investigate the effect of hydration. The optimized configurations of the hydrated clusters and the stepwise hydration free energy are presented in Figure S9 and Table S3, respectively. The equilibrium hydrate distribution at 278.15 K and relative humidity (RH) of 20%, 50%, and 80% are presented in Figure S10. Figure S10 shows that all heteromolecular clusters except $(MEA)_1(MSA)_1$ and $(MEA)_2(MSA)_2$ are predominantly hydrated by one or two H_2O molecules, and all homomolecular clusters except MSA are barely hydrated at all the studied RHs. $(MEA)_1(MSA)_1$ and $(MEA)_2(MSA)_2$ can be hydrated by three H_2O molecules and MSA by one H_2O molecule, which implies that clusters with an equal amount of acid and base molecules are more hydrophilic. Therefore, it can be concluded that the MEA−MSA clusters can be mildly hydrated with one to three H_2O molecules depending on RH.

The relative evaporation rate and cluster formation rate as a function of RH at 278.15 K compared to dry conditions are presented in Figure 6. The effect of hydration depends on the cluster composition for the $(MEA)_m(MSA)_n$ (m = 0−2, n = 0−2) clusters. The evaporation rates of $(MEA)_2$ and $(MEA)_2(MSA)_2$ are almost unchanged, and $(MSA)_2$ is slightly increased by hydration. However, the evaporation rates of the $(MEA)_1(MSA)_2$ and $(MEA)_2(MSA)_1$ clusters were found to increase by up to 8 and 14 times by hydration, respectively. More importantly, hydration significantly decreases the evaporation rate (up to 50 times compared to the dry condition) of the initially formed $(MEA)_1(MSA)_1$ cluster, which was shown to be the rate-determining step for the cluster growth in the system. The decreased evaporation rate of the $(MEA)_1(MSA)_1$ cluster is the main reason that the cluster formation rate is significant increased (up to 18 times, right panel in Figure 6), and $(MEA)_1(MSA)_1$ contributes more to the initially formed clusters compared to the anhydration case (Figure S11). Note that the relative formation rate presented here should cancel out any significant bias introduced by the smaller "2 × 2 box" size. Generally, from these small cluster hydration simulations, we can conclude that hydration can significantly affect the cluster formation rates. This is different from the SA−amine (MA, DMA, and MEA) cluster systems, in which hydration has little effect on the cluster formation rates.[11] We note that the experiments from Finlayson-Pitts group showed that an increase in the RH greatly increased the nucleation rate of the MSA−base (base = ammonia, MA, DMA and TMA) clusters,[41] which is similar to our findings.

Uncertainty Analysis of ACDC Simulations. Here, the potential uncertainties arising from the manner that ACDC is calculating the collision rate coefficients are analyzed. We also investigate how variable settings, such as the sticking factor and coagulation sink coefficient, affect the main results. Since the cluster formation process does not involve chemical reaction energy barriers,[82] ACDC employs kinetic gas theory to calculate the collision rate coefficients by assuming that all colliding molecules follow hard-sphere collisions; i.e., there is no specific interaction between the colliding molecules. We noted that recent studies by Lin et al. and Lee et al. argued that the dipole−dipole interaction between colliding molecules could play an important role in enhancing collision rates.[83,84] To address the possible uncertainty resulting from kinetic gas theory, we employed the long-range transition state theory with a dipole−dipole force potential and the statistical adiabatic channel model[85,86] as test methods to calculate the collision rate coefficients between monomers in MEA−MSA and MA−MSA cluster systems at 278.15 K. Both theories explicitly consider dipole−dipole interactions between the molecules (see the Computational Details for Collision Rate Coefficients from Test Methods section in the SI). As can be seen in Table S7, there is a maximum of about 2 times difference in the collision rate coefficients between the two test methods and kinetic gas theory. Therefore, kinetic gas theory employed in ACDC should provide reasonable collision rate coefficients for the MEA−MSA and MA−MSA cluster systems. In addition, both the sticking factor and coagulation sink coefficient can affect the enhancing potential (the concentration of $\Sigma(MSA)_2$ and cluster formation rates) of MEA and MA on MSA-driven NPF (detailed discussion in the SI). However, within all of the considered change ranges of the coagulation sink coefficient and sticking factor, the enhancing potential of MEA is still significantly higher than that of MA.

Atmospheric Implications. This study reveals that MEA has a higher enhancing potential than MA, the previously known strongest enhancing agent,[41,42] on MSA-driven NPF. Therefore, at a similar atmospheric concentration to MA, MEA can significantly enhance MSA-driven NPF. Considering the high production of MEA and the detection of MEA in the particle phase at various locations,[52,56,57] MEA could be an important contributor to MSA-driven NPF in locations with high MEA and MSA concentrations. Especially, with the large-scale implementation of MEA-based PCCC, MEA will play a more important role in MSA-driven NPF in the future. Therefore, more studies on the atmospheric concentration detection of MEA and the participation of MEA in MSA-driven NPF is warranted.

This study found that a high gas-phase basicity and additional H-bonding capacity from the nonamino group are both important factors for the higher enhancing potential of MEA compared to MA. We note that the gas-phase basicity of DMA is similar to MEA;[43] however, its enhancing potential on MSA-driven NPF is much lower than that of MEA.[41] Therefore, the H-bonding capacity of MEA plays an important role in determining its enhancing potential. In addition, this study is the first to point out that the H-bonding capacity of the nonamino group plays an important role in determining the enhancing potential of amines on MSA-based NPF. In the atmosphere, many bases have a high gas-phase basicity and H-bonding capacity from nonamino groups, e.g., diamines and amino acids. Moreover, highly oxygenated multifunctional molecules (HOMs) with an amino group could also contribute to MSA-based NPF due to their high H-bonding capacity.[87,88] Therefore, the enhancing potential of diamine, amino acid, and HOMs with an amino group on MSA-driven NPF deserves future investigation to comprehensively understand the contribution of MSA on NPF.

■ ASSOCIATED CONTENT

Supporting Information

The Supporting Information is available free of charge at https://pubs.acs.org/doi/10.1021/acs.est.9b05306.

Details for judging of cluster stability and boundary conditions, effect of temperature, effect of variables

DOI: 10.1021/acs.est.9b05306
Environ. Sci. Technol. 2019, 53, 14387−14397

settings of ACDC, effect of hydration on cluster formation pathways, computational details for collision rate coefficients from test methods, thermodynamics information for the formation of molecular clusters, evaporation coefficients for all evaporation pathways of different clusters, hydration free energies, conformations of MA−MSA clusters and hydrate MEA−MSA clusters, the main clustering pathways for MA−MSA clusters, comparison for steady-state MSA dimer concentration and the cluster formation rate with a "2 × 2 box" simulation between MEA−MSA and the MA−MSA system, hydration distribution of clusters, and coordinates of all optimized clusters. (PDF)

AUTHOR INFORMATION

Corresponding Author

*Phone/Fax: +86-411-84707251. E-mail: hbxie@dlut.edu.cn.

ORCID

Hong-Bin Xie: 0000-0002-9119-9785

Jonas Elm: 0000-0003-3736-4329

Jingwen Chen: 0000-0002-5756-3336

Hanna Vehkamäki: 0000-0002-5018-1255

Notes

The authors declare no competing financial interest.

ACKNOWLEDGMENTS

The study was supported by the National Natural Science Foundation of China (21876024, 21677028), the Major International (Regional) Joint Research Project (21661142001), the Program for Changjiang Scholars and Innovative Research Team in University (IRT_13R05), the Programme of Introducing Talents of Discipline to Universities (B13012), the Supercomputing Center of Dalian University of Technology, ERC Project 692891-DAMOCLES, the Academy of Finland, and the University of Helsinki, Faculty of Science ATMATH Project.

REFERENCES

(1) Yao, L.; Garmash, O.; Bianchi, F.; Zheng, J.; Yan, C.; Kontkanen, J.; Junninen, H.; Mazon, S. B.; Ehn, M.; Paasonen, P.; Sipila, M.; Wang, M. Y.; Wang, X. K.; Xiao, S.; Chen, H. F.; Lu, Y. Q.; Zhang, B. W.; Wang, D. F.; Fu, Q. Y.; Geng, F. H.; Li, L.; Wang, H. L.; Qiao, L. P.; Yang, X.; Chen, J. M.; Kerminen, V. M.; Petaja, T.; Worsnop, D. R.; Kulmala, M.; Wang, L. Atmospheric New Particle Formation from Sulfuric Acid and Amines in A Chinese Megacity. *Science* **2018**, *361* (6399), 278.

(2) Olenius, T.; Halonen, R.; Kurtén, T.; Henschel, H.; Kupiainen-Määttä, O.; Ortega, I. K.; Jen, C. N.; Vehkamäki, H.; Riipinen, I. New particle formation from sulfuric acid and amines: Comparison of monomethylamine, dimethylamine, and trimethylamine. *J. Geophys. Res.-Atmos.* **2017**, *122* (13), 7103−7118.

(3) Almeida, J.; Schobesberger, S.; Kurtén, A.; Ortega, I. K.; Kupiainen-Maatta, O.; Praplan, A. P.; Adamov, A.; Amorim, A.; Bianchi, F.; Breitenlechner, M.; David, A.; Dommen, J.; Donahue, N. M.; Downard, A.; Dunne, E.; Duplissy, J.; Ehrhart, S.; Flagan, R. C.; Franchin, A.; Guida, R.; Hakala, J.; Hansel, A.; Heinritzi, M.; Henschel, H.; Jokinen, T.; Junninen, H.; Kajos, M.; Kangasluoma, J.; Keskinen, H.; Kupc, A.; Kurtén, T.; Kvashin, A. N.; Laaksonen, A.; Lehtipalo, K.; Leiminger, M.; Leppa, J.; Loukonen, V.; Makhmutov, V.; Mathot, S.; McGrath, M. J.; Nieminen, T.; Olenius, T.; Onnela, A.; Petaja, T.; Riccobono, F.; Riipinen, I.; Rissanen, M.; Rondo, L.; Ruuskanen, T.; Santos, F. D.; Sarnela, N.; Schallhart, S.; Schnitzhofer, R.; Seinfeld, J. H.; Simon, M.; Sipila, M.; Stozhkov, Y.; Stratmann, F.; Tome, A.; Trostl, J.; Tsagkogeorgas, G.; Vaattovaara, P.; Viisanen, Y.; Virtanen, A.; Vrtala, A.; Wagner, P. E.; Weingartner, E.; Wex, H.; Williamson, C.; Wimmer, D.; Ye, P.; Yli-Juuti, T.; Carslaw, K. S.; Kulmala, M.; Curtius, J.; Baltensperger, U.; Worsnop, D. R.; Vehkamäki, H.; Kirkby, J. Molecular Understanding of Sulphuric Acid-amine Particle Nucleation in the Atmosphere. *Nature* **2013**, *502* (7471), 359−363.

(4) Kirkby, J.; Curtius, J.; Almeida, J.; Dunne, E.; Duplissy, J.; Ehrhart, S.; Franchin, A.; Gagne, S.; Ickes, L.; Kurten, A.; Kupc, A.; Metzger, A.; Riccobono, F.; Rondo, L.; Schobesberger, S.; Tsagkogeorgas, G.; Wimmer, D.; Amorim, A.; Bianchi, F.; Breitenlechner, M.; David, A.; Dommen, J.; Downard, A.; Ehn, M.; Flagan, R. C.; Haider, S.; Hansel, A.; Hauser, D.; Jud, W.; Junninen, H.; Kreissl, F.; Kvashin, A.; Laaksonen, A.; Lehtipalo, K.; Lima, J.; Lovejoy, E. R.; Makhmutov, V.; Mathot, S.; Mikkila, J.; Minginette, P.; Mogo, S.; Nieminen, T.; Onnela, A.; Pereira, P.; Petaja, T.; Schnitzhofer, R.; Seinfeld, J. H.; Sipila, M.; Stozhkov, Y.; Stratmann, F.; Tome, A.; Vanhanen, J.; Viisanen, Y.; Vrtala, A.; Wagner, P. E.; Walther, H.; Weingartner, E.; Wex, H.; Winkler, P. M.; Carslaw, K. S.; Worsnop, D. R.; Baltensperger, U.; Kulmala, M. Role of Sulphuric Acid, Ammonia and Galactic Cosmic Rays in Atmospheric Aerosol Nucleation. *Nature* **2011**, *476* (7361), 429−33.

(5) Zhang, R. Y.; Suh, I.; Zhao, J.; Zhang, D.; Fortner, E. C.; Tie, X. X.; Molina, L. T.; Molina, M. J. Atmospheric New Particle Formation Enhanced by Organic Acids. *Science* **2004**, *304* (5676), 1487−1490.

(6) Winkler, P. M.; Steiner, G.; Vrtala, A.; Vehkamäki, H.; Noppel, M.; Lehtinen, K. E. J.; Reischl, G. P.; Wagner, P. E.; Kulmala, M. Heterogeneous Nucleation Experiments Bridging the Scale from Molecular Ion Clusters to Nanoparticles. *Science* **2008**, *319* (5868), 1374−1377.

(7) Ehn, M.; Thornton, J. A.; Kleist, E.; Sipila, M.; Junninen, H.; Pullinen, I.; Springer, M.; Rubach, F.; Tillmann, R.; Lee, B.; Lopez-Hilfiker, F.; Andres, S.; Acir, I.-H.; Rissanen, M.; Jokinen, T.; Schobesberger, S.; Kangasluoma, J.; Kontkanen, J.; Nieminen, T.; Kurtén, T.; Nielsen, L. B.; Jorgensen, S.; Kjaergaard, H. G.; Canagaratna, M.; Dal Maso, M.; Berndt, T.; Petaja, T.; Wahner, A.; Kerminen, V.-M.; Kulmala, M.; Worsnop, D. R.; Wildt, J.; Mentel, T. F. A Large Source of Low-volatility Secondary Organic Aerosol. *Nature* **2014**, *506* (7489), 476−479.

(8) Wang, Y. H.; Liu, Z. R.; Zhang, J. K.; Hu, B.; Ji, D. S.; Yu, Y. C.; Wang, Y. S. Aerosol Physicochemical Properties and Implications for Visibility During an Intense Haze Episode During Winter in Beijing. *Atmos. Chem. Phys.* **2015**, *15* (6), 3205−3215.

(9) Rose, C.; Zha, Q.; Dada, L.; Yan, C.; Lehtipalo, K.; Junninen, H.; Mazon, S. B.; Jokinen, T.; Sarnela, N.; Sipila, M.; Petaja, T.; Kerminen, V. M.; Bianchi, F.; Kulmala, M. Observations of Biogenic Ion-induced Cluster Formation in the Atmosphere. *Sci. Adv.* **2018**, *4* (4), No. eaar5218.

(10) Xu, J.; Perraud, V.; Finlayson-Pitts, B. J.; Gerber, R. B. Uptake of Water by an Acid-base Nanoparticle: Theoretical and Experimental Studies of the Methanesulfonic Acid-methylamine System. *Phys. Chem. Chem. Phys.* **2018**, *20* (34), 22249−22259.

(11) Xie, H. B.; Elm, J.; Halonen, R.; Myllys, N.; Kurtén, T.; Kulmala, M.; Vehkamäki, H. Atmospheric Fate of Monoethanolamine: Enhancing New Particle Formation of Sulfuric Acid as an Important Removal Process. *Environ. Sci. Technol.* **2017**, *51* (15), 8422−8431.

(12) Kurtén, T.; Loukonen, V.; Vehkamäki, H.; Kulmala, M. Amines Are Likely to Enhance Neutral and Ion-induced Sulfuric Acid-water Nucleation in the Atmosphere More Effectively than Ammonia. *Atmos. Chem. Phys.* **2008**, *8* (14), 4095−4103.

(13) Loukonen, V.; Kurtén, T.; Ortega, I. K.; Vehkamäki, H.; Pádua, A. A. H.; Sellegri, K.; Kulmala, M. Enhancing Effect of Dimethylamine in Sulfuric Acid Nucleation in the Presence of Water − A Computational Study. *Atmos. Chem. Phys.* **2010**, *10* (10), 4961−4974.

(14) Murphy, S. M.; Sorooshian, A.; Kroll, J. H.; Ng, N. L.; Chhabra, P.; Tong, C.; Surratt, J. D.; Knipping, E.; Flagan, R. C.; Seinfeld, J. H. Secondary Aerosol Formation from Atmospheric Reactions of Aliphatic Amines. *Atmos. Chem. Phys.* **2007**, *7* (9), 2313−2337.

DOI: 10.1021/acs.est.9b05306
Environ. Sci. Technol. 2019, 53, 14387−14397

(15) Smith, J. N.; Barsanti, K. C.; Friedli, H. R.; Ehn, M.; Kulmala, M.; Collins, D. R.; Scheckman, J. H.; Williams, B. J.; McMurry, P. H. Observations of Aminium Salts in Atmospheric Nanoparticles and Possible Climatic Implications. *Proc. Natl. Acad. Sci. U. S. A.* **2010**, *107* (15), 6634−6639.
(16) Zhao, J.; Smith, J. N.; Eisele, F. L.; Chen, M.; Kuang, C.; McMurry, P. H. Observation of Neutral Sulfuric Acid-amine Containing Clusters in Laboratory and Ambient Measurements. *Atmos. Chem. Phys.* **2011**, *11* (21), 10823−10836.
(17) Erupe, M. E.; Viggiano, A. A.; Lee, S. H. The Effect of Trimethylamine on Atmospheric Nucleation Involving H_2SO_4. *Atmos. Chem. Phys.* **2011**, *11* (10), 4767−4775.
(18) Lehtipalo, K.; Rondo, L.; Kontkanen, J.; Schobesberger, S.; Jokinen, T.; Sarnela, N.; Kuerten, A.; Ehrhart, S.; Franchin, A.; Nieminen, T.; Riccobono, F.; Sipila, M.; Yli-Juuti, T.; Duplissy, J.; Adamov, A.; Ahlm, L.; Almeida, J.; Amorim, A.; Bianchi, F.; Breitenlechner, M.; Dommen, J.; Downard, A. J.; Dunne, E. M.; Flagan, R. C.; Guida, R.; Hakala, J.; Hansel, A.; Jud, W.; Kangasluoma, J.; Kerminen, V.-M.; Keskinen, H.; Kim, J.; Kirkby, J.; Kupc, A.; Kupiainen-Maatta, O.; Laaksonen, A.; Lawler, M. J.; Leiminger, M.; Mathot, S.; Olenius, T.; Ortega, I. K.; Onnela, A.; Petaja, T.; Praplan, A.; Rissanen, M. P.; Ruuskanen, T.; Santos, F. D.; Schallhart, S.; Schnitzhofer, R.; Simon, M.; Smith, J. N.; Trostl, J.; Tsagkogeorgas, G.; Tome, A.; Vaattovaara, P.; Vehkamäki, H.; Vrtala, A. E.; Wagner, P. E.; Williamson, C.; Wimmer, D.; Winkler, P. M.; Virtanen, A.; Donahue, N. M.; Carslaw, K. S.; Baltensperger, U.; Riipinen, I.; Curtius, J.; Worsnop, D. R.; Kulmala, M. The Effect of Acid-base Clustering and Ions on the Growth of Atmospheric Nano-particles. *Nat. Commun.* **2016**, *7*, 11594.
(19) Chen, M.; Titcombe, M.; Jiang, J.; Jen, C.; Kuang, C.; Fischer, M. L.; Eisele, F. L.; Siepmann, J. I.; Hanson, D. R.; Zhao, J.; McMurry, P. H. Acid-base Chemical Reaction Model for Nucleation Rates in the Polluted Atmospheric Boundary Layer. *Proc. Natl. Acad. Sci. U. S. A.* **2012**, *109* (46), 18713−18718.
(20) Lv, S.-S.; Miao, S.-K.; Ma, Y.; Zhang, M.-M.; Wen, Y.; Wang, C.-Y.; Zhu, Y.-P.; Huang, W. Properties and Atmospheric Implication of Methylamine-Sulfuric Acid-Water Clusters. *J. Phys. Chem. A* **2015**, *119* (32), 8657−8666.
(21) Sipila, M.; Berndt, T.; Petaja, T.; Brus, D.; Vanhanen, J.; Stratmann, F.; Patokoski, J.; Mauldin, R. L.; Hyvarinen, A. P.; Lihavainen, H.; Kulmala, M. The Role of Sulfuric Acid in Atmospheric Nucleation. *Science* **2010**, *327* (5970), 1243−1246.
(22) Nadykto, A. B.; Yu, F.; Jakovleva, M. V.; Herb, J.; Xu, Y. Amines in the Earth's Atmosphere: A Density Functional Theory Study of the Thermochemistry of Pre-Nucleation Clusters. *Entropy* **2011**, *13* (2), 554−569.
(23) Nadykto, A.; Herb, J.; Yu, F.; Xu, Y.; Nazarenko, E. Estimating the Lower Limit of the Impact of Amines on Nucleation in the Earth's Atmosphere. *Entropy* **2015**, *17* (5), 2764−2780.
(24) Nadykto, A. B.; Herb, J.; Yu, F.; Xu, Y. Enhancement in the Production of Nucleating Clusters due to Dimethylamine and Large Uncertainties in the Thermochemistry of Amine-enhanced Nucleation. *Chem. Phys. Lett.* **2014**, *609*, 42−49.
(25) Jen, C. N.; McMurry, P. H.; Hanson, D. R. Stabilization of Sulfuric Acid Dimers by Ammonia, Methylamine, Dimethylamine, and Trimethylamine. *J. Geophys. Res.: Atmos.* **2014**, *119* (12), 7502−7514.
(26) Qiu, C.; Zhang, R. Y. Multiphase Chemistry of Atmospheric Amines. *Phys. Chem. Chem. Phys.* **2013**, *15* (16), 5738−5752.
(27) Zhang, R.; Wang, L.; Khalizov, A. F.; Zhao, J.; Zheng, J.; McGraw, R. L.; Molina, L. T. Formation of Nanoparticles of Blue Haze Enhanced by Anthropogenic Pollution. *Proc. Natl. Acad. Sci. U. S. A.* **2009**, *106* (42), 17650−17654.
(28) Xu, W.; Zhang, R. Y. A Theoretical Study of Hydrated Molecular Clusters of Amines and Dicarboxylic Acids. *J. Chem. Phys.* **2013**, *139* (6), 064312.
(29) Dawson, M. L.; Varner, M. E.; Perraud, V.; Ezell, M. J.; Gerber, R. B.; Finlayson-Pitts, B. J. Simplified Mechanism for New Particle Formation from Methanesulfonic Acid, Amines, and Water via Experiments and ab initio Calculations. *Proc. Natl. Acad. Sci. U. S. A.* **2012**, *109* (46), 18719−18724.
(30) Wehner, B.; Petäjä, T.; Boy, M.; Engler, C.; Birmili, W.; Tuch, T.; Wiedensohler, A.; Kulmala, M. The Contribution of Sulfuric Acid and Non-volatile Compounds on the Growth of Freshly Formed Atmospheric Aerosols. *Geophys. Res. Lett.* **2005**, *32* (17), L17810.
(31) Kirkby, J.; Duplissy, J.; Sengupta, K.; Frege, C.; Gordon, H.; Williamson, C.; Heinritzi, M.; Simon, M.; Yan, C.; Almeida, J.; Trostl, J.; Nieminen, T.; Ortega, I. K.; Wagner, R.; Adamov, A.; Amorim, A.; Bernhammer, A. K.; Bianchi, F.; Breitenlechner, M.; Brilke, S.; Chen, X. M.; Craven, J.; Dias, A.; Ehrhart, S.; Flagan, R. C.; Franchin, A.; Fuchs, C.; Guida, R.; Hakala, J.; Hoyle, C. R.; Jokinen, T.; Junninen, H.; Kangasluoma, J.; Kim, J.; Krapf, M.; Kurten, A.; Laaksonen, A.; Lehtipalo, K.; Makhmutov, V.; Mathot, S.; Molteni, U.; Onnela, A.; Perakyla, O.; Piel, F.; Petaja, T.; Praplan, A. P.; Pringle, K.; Rap, A.; Richards, N. A. D.; Riipinen, I.; Rissanen, M. P.; Rondo, L.; Sarnela, N.; Schobesberger, S.; Scott, C. E.; Seinfeld, J. H.; Sipila, M.; Steiner, G.; Stozhkov, Y.; Stratmann, F.; Tome, A.; Virtanen, A.; Vogel, A. L.; Wagner, A. C.; Wagner, P. E.; Weingartner, E.; Wimmer, D.; Winkler, P. M.; Ye, P. L.; Zhang, X.; Hansel, A.; Dommen, J.; Donahue, N. M.; Worsnop, D. R.; Baltensperger, U.; Kulmala, M.; Carslaw, K. S.; Curtius, J. Ion-induced Nucleation of Pure Biogenic Particles. *Nature* **2016**, *533* (7604), 521−526.
(32) Bianchi, F.; Trostl, J.; Junninen, H.; Frege, C.; Henne, S.; Hoyle, C. R.; Molteni, U.; Herrmann, E.; Adamov, A.; Bukowiecki, N.; Chen, X.; Duplissy, J.; Gysel, M.; Hutterli, M.; Kangasluoma, J.; Kontkanen, J.; Kurten, A.; Manninen, H. E.; Munch, S.; Perakyla, O.; Petaja, T.; Rondo, L.; Williamson, C.; Weingartner, E.; Curtius, J.; Worsnop, D. R.; Kulmala, M.; Dommen, J.; Baltensperger, U. New Particle Formation in the Free Troposphere: A Question of Chemistry and Timing. *Science* **2016**, *352* (6289), 1109−1112.
(33) Perraud, V.; Horne, J. R.; Martinez, A. S.; Kalinowski, J.; Meinardi, S.; Dawson, M. L.; Wingen, L. M.; Dabdub, D.; Blake, D. R.; Gerber, R. B.; Finlayson-Pitts, B. J. The Future of Airborne Sulfur-containing Particles in the Absence of Fossil Fuel Sulfur Dioxide Emissions. *Proc. Natl. Acad. Sci. U. S. A.* **2015**, *112* (44), 13514−13519.
(34) Hodshire, A. L.; Campuzano-Jost, P.; Kodros, J. K.; Croft, B.; Nault, B. A.; Schroder, J. C.; Jimenez, J. L.; Pierce, J. R. The Potential Role of Methanesulfonic Acid (MSA) in Aerosol Formation and Growth and the Associated Radiative Forcings. *Atmos. Chem. Phys.* **2019**, *19* (5), 3137−3160.
(35) Hopkins, R. J.; Desyaterik, Y.; Tivanski, A. V.; Zaveri, R. A.; Berkowitz, C. M.; Tyliszczak, T.; Gilles, M. K.; Laskin, A. Chemical Speciation of Sulfur in Marine Cloud Droplets and Particles: Analysis of Individual Particles from the Marine Boundary Layer over the California Current. *J. Geophys. Res.* **2008**, *113* (D4), 209 (1−15).
(36) Arquero, K. D.; Xu, J.; Gerber, R. B.; Finlayson-Pitts, B. J. Particle Formation and Growth from Oxalic Acid, Methanesulfonic Acid, Trimethylamine and Water: a Combined Experimental and Theoretical Study. *Phys. Chem. Chem. Phys.* **2017**, *19* (41), 28286−28301.
(37) Stern, D. I. Global Sulfur Emissions from 1850 to 2000. *Chemosphere* **2005**, *58* (2), 163−175.
(38) Barnes, I.; Hjorth, J.; Mihalopoulos, N. Dimethyl Sulfide and Dimethyl Sulfoxide and Their Oxidation in the Atmosphere. *Chem. Rev.* **2006**, *106* (3), 940−975.
(39) Eisele, F. L.; Tanner, D. J. Measurement of the Gas Phase Concentration of H_2SO_4 and Methane Sulfonic Acid and Estimates of H_2SO_4 Production and Loss in the Atmosphere. *J. Geophys. Res.-Atmos.* **1993**, *98* (D5), 9001−9010.
(40) Berresheim, H. E.T.; Tremmel, H. G.; Allen, A. G.; Hansson, H. C.; Rosman, K.; Dal Maso, M.; Mäkelä, J. M.; Kulmala, M.; O'Dowd, C. D. Gas-aerosol Relationships of H_2SO_4, MSA, and OH: Observations in the Coastal Marine Boundary Layer at Mace Head, Ireland. *J. Geophys. Res.-Atmos.* **2002**, *107* (D19), PAR5−1−PAR 5−12.
(41) Chen, H.; Varner, M. E.; Gerber, R. B.; Finlayson-Pitts, B. J. Reactions of Methanesulfonic Acid with Amines and Ammonia as a

DOI: 10.1021/acs.est.9b05306
Environ. Sci. Technol. 2019, 53, 14387−14397

Source of New Particles in Air. *J. Phys. Chem. B* **2016**, *120* (8), 1526−1536.
(42) Chen, H.; Finlayson-Pitts, B. J. New Particle Formation from Methanesulfonic Acid and Amines/Ammonia as a Function of Temperature. *Environ. Sci. Technol.* **2017**, *51* (1), 243−252.
(43) Hunter, E. P. L.; Lias, S. G. Evaluated Gas Phase Basicities and Proton Affinities of Molecules: An Update. *J. Phys. Chem. Ref. Data* **1998**, *27* (3), 413−656.
(44) Yang, Y.; Waller, S. E.; Kreinbihl, J. J.; Johnson, C. J. Direct Link between Structure and Hydration in Ammonium and Aminium Bisulfate Clusters Implicated in Atmospheric New Particle Formation. *J. Phys. Chem. Lett.* **2018**, *9* (18), 5647−5652.
(45) Waller, S. E.; Yang, Y.; Castracane, E.; Racow, E. E.; Kreinbihl, J. J.; Nickson, K. A.; Johnson, C. J. The Interplay Between Hydrogen Bonding and Coulombic Forces in Determining the Structure of Sulfuric Acid-Amine Clusters. *J. Phys. Chem. Lett.* **2018**, *9* (6), 1216−1222.
(46) Xie, H.-B.; He, N.; Song, Z.; Chen, J.; Li, X. Theoretical Investigation on the Different Reaction Mechanisms of Aqueous 2-Amino-2-methyl-1-propanol and Monoethanolamine with CO_2. *Ind. Eng. Chem. Res.* **2014**, *53* (8), 3363−3372.
(47) Puxty, G.; Rowland, R.; Allport, A.; Yang, Q.; Bown, M.; Burns, R.; Maeder, M.; Attalla, M. Carbon Dioxide Postcombustion Capture: A Novel Screening Study of the Carbon Dioxide Absorption Performance of 76 Amines. *Environ. Sci. Technol.* **2009**, *43* (16), 6427−6433.
(48) Veawab, A.; Tontiwachwuthikul, P.; Chakma, A. Corrosion Behavior of Carbon Steel in the CO_2 Absorption Process Using Aqueous Amine Solutions. *Ind. Eng. Chem. Res.* **1999**, *38* (10), 3917−3924.
(49) Liu, Y. D.; Zhang, L. Z.; Watanasiri, S. Representing Vapor-liquid Equilibrium for an Aqueous MEA-CO_2 system Using the Electrolyte Nonrandom-two-liquid Model. *Ind. Eng. Chem. Res.* **1999**, *38* (5), 2080−2090.
(50) Xie, H. B.; Zhou, Y.; Zhang, Y.; Johnson, J. K. Reaction Mechanism of Monoethanolamine with CO_2 in Aqueous Solution from Molecular Modeling. *J. Phys. Chem. A* **2010**, *114* (43), 11844−11852.
(51) da Silva, E. F.; Booth, A. M. Emissions from Postcombustion CO_2 Capture Plants. *Environ. Sci. Technol.* **2013**, *47* (2), 659−660.
(52) McDonald, B. C.; de Gouw, J. A.; Gilman, J. B.; Jathar, S. H.; Akherati, A.; Cappa, C. D.; Jimenez, J. L.; Lee-Taylor, J.; Hayes, P. L.; McKeen, S. A.; Cui, Y. Y.; Kim, S. W.; Gentner, D. R.; Isaacman-VanWertz, G.; Goldstein, A. H.; Harley, R. A.; Frost, G. J.; Roberts, J. M.; Ryerson, T. B.; Trainer, M. Volatile Chemical Products Emerging as Largest Petrochemical Source of Urban Organic Emissions. *Science* **2018**, *359* (6377), 760−764.
(53) Karl, M.; Wright, R. F.; Berglen, T. F.; Denby, B. Worst Case Scenario Study to Assess the Environmental Impact of Amine Emissions from a CO_2 Capture Plant. *Int. J. Greenhouse Gas Control* **2011**, *5* (3), 439−447.
(54) Veltman, K.; Singh, B.; Hertwich, E. G. Human and Environmental Impact Assessment of Postcombustion CO_2 Capture Focusing on Emissions from Amine-Based Scrubbing Solvents to Air. *Environ. Sci. Technol.* **2010**, *44* (4), 1496−1502.
(55) Kapteina, S.; Slowik, K.; Verevkin, S. P.; Heintz, A. Vapor Pressures and Vaporization Enthalpies of a Series of Ethanolamines. *J. Chem. Eng. Data* **2005**, *50* (2), 398−402.
(56) Huang, X. F.; Deng, C. R.; Zhuang, G. S.; Lin, J.; Xiao, M. X. Quantitative Analysis of Aliphatic Amines in Urban Aerosols Based on Online Derivatization and High Performance Liquid Chromatography. *Environ. Sci.: Process Impacts* **2016**, *18* (7), 796−801.
(57) Borduas, N.; Abbatt, J. P. D.; Murphy, J. G. Gas Phase Oxidation of Monoethanolamine (MEA) with OH Radical and Ozone: Kinetics, Products, and Particles. *Environ. Sci. Technol.* **2013**, *47* (12), 6377−6383.
(58) Zhang, Q.; Anastasio, C. Free and Combined Amino Compounds in Atmospheric Fine Particles (PM2.5) and Fog Waters from Northern California. *Atmos. Environ.* **2003**, *37* (16), 2247−2258.
(59) McGrath, M. J.; Olenius, T.; Ortega, I. K.; Loukonen, V.; Paasonen, P.; Kurtén, T.; Kulmala, M.; Vehkamäki, H. Atmospheric Cluster Dynamics Code: a flexible method for solution of the birthdeath equations. *Atmos. Chem. Phys.* **2012**, *12* (5), 2345−2355.
(60) Elm, J.; Jen, C. N.; Kurtén, T.; Vehkamäki, H. Strong Hydrogen Bonded Molecular Interactions between Atmospheric Diamines and Sulfuric Acid. *J. Phys. Chem. A* **2016**, *120* (20), 3693−3700.
(61) Elm, J.; Fard, M.; Bilde, M.; Mikkelsen, K. V. Interaction of Glycine with Common Atmospheric Nucleation Precursors. *J. Phys. Chem. A* **2013**, *117* (48), 12990−12997.
(62) Elm, J.; Myllys, N.; Hyttinen, N.; Kurtén, T. Computational Study of the Clustering of a Cyclohexene Autoxidation Product $C_6H_8O_7$ with Itself and Sulfuric Acid. *J. Phys. Chem. A* **2015**, *119* (30), 8414−8421.
(63) Ma, F. F.; Xie, H. B.; Elm, J.; Shen, J. W.; Chen, J. W.; Vehkamäki, H. Piperazine Enhancing Sulfuric Acid-Based New Particle Formation: Implications for the Atmospheric Fate of Piperazine. *Environ. Sci. Technol.* **2019**, *53* (15), 8785−8795.
(64) Frisch, M. J.; Trucks, G. W.; Schlegel, H. B.; Scuseria, G. E.; Robb, M. A.; Cheeseman, J. R.; Scalmani, G.; Barone, V.; Mennucci, B.; Petersson, G. A.; Nakatsuji, H.; Caricato, M.; Li, X.; Hratchian, H. P.; Izmaylov, A. F.; Bloino, J.; Zheng, G.; Sonnenberg, J. L.; Hada, M.; Ehara, M.; Toyota, K.; Fukuda, R.; Hasegawa, J.; Ishida, M.; Nakajima, T.; Honda, Y.; Kitao, O.; Nakai, H.; Vreven, T.; Montgomery, J. A., Jr.; Peralta, P. E.; Ogliaro, F.; Bearpark, M.; Heyd, J. J.; Brothers, E.; Kudin, K. N.; Staroverov, V. N.; Kobayashi, R.; Normand, J.; Raghavachari, K.; Rendell, A.; Burant, J. C.; Iyengar, S. S.; Tomasi, J.; Cossi, M.; Rega, N.; Millam, N. J.; Klene, M.; Knox, J. E.; Cross, J. B.; Bakken, V.; Adamo, C.; Jaramillo, J.; Gomperts, R.; Stratmann, R. E.; Yazyev, O.; Austin, A. J.; Cammi, R.; Pomelli, C.; Ochterski, J. W.; Martin, R. L.; Morokuma, K.; Zakrzewski, V. G.; Voth, G. A.; Salvador, P.; Dannenberg, J. J.; Dapprich, S.; Daniels, A. D.; Farkas, Ö.; Ortiz, J. V.; Cioslowski, J.; Fox, D. J. *Gaussian 09* ; Gaussian, Inc.: Wallingford, CT, 2009
(65) Neese, F. The ORCA program system. *Wiley Interdiscip. Rev. Comput. Mol. Sci.* **2012**, *2* (1), 73−78.
(66) Elm, J.; Bilde, M.; Mikkelsen, K. V. Assessment of binding energies of atmospherically relevant clusters. *Phys. Chem. Chem. Phys.* **2013**, *15* (39), 16442−16445.
(67) Elm, J.; Kristensen, K. Basis Set Convergence of the Binding Energies of Strongly Hydrogen-bonded Atmospheric Clusters. *Phys. Chem. Chem. Phys.* **2017**, *19* (2), 1122−1133.
(68) Myllys, N.; Elm, J.; Halonen, R.; Kurtén, T.; Vehkamäki, H. Coupled Cluster Evaluation of the Stability of Atmospheric Acid-Base Clusters with up to 10 Molecules. *J. Phys. Chem. A* **2016**, *120* (4), 621−630.
(69) Riplinger, C.; Sandhoefer, B.; Hansen, A.; Neese, F. Natural Triple Excitations in Local Coupled Cluster Calculations with Pair Natural Orbitals. *J. Chem. Phys.* **2013**, *139* (13), 134101.
(70) Riplinger, C.; Neese, F. An Efficient and Near Linear Scaling Pair Natural Orbital Based Local Coupled Cluster Method. *J. Chem. Phys.* **2013**, *138* (3), 034106.
(71) Kumar, M.; Francisco, J. S. Ion Pair Particles at the Air-water Interface. *Proc. Natl. Acad. Sci. U. S. A.* **2017**, *114* (47), 12401−12406.
(72) Xu, J.; Finlayson-Pitts, B. J.; Gerber, R. B. Proton Transfer in Mixed Clusters of Methanesulfonic Acid, Methylamine, and Oxalic Acid: Implications for Atmospheric Particle Formation. *J. Phys. Chem. A* **2017**, *121* (12), 2377−2385.
(73) Olenius, T.; Kupiainen-Maatta, O.; Ortega, I. K.; Kurtén, T.; Vehkamäki, H. Free Energy Barrier in the Growth of Sulfuric Acid-ammonia and Sulfuric Acid-dimethylamine Clusters. *J. Chem. Phys.* **2013**, *139* (8), 084312.
(74) Dal Maso, M.; Hyvarinen, A.; Komppula, M.; Tunved, P.; Kerminen, V. M.; Lihavainen, H.; Viisanen, Y.; Hansson, H. C.; Kulmala, M. Annual and Interannual Variation in Boreal Forest Aerosol Particle Number and Volume Concentration and Their Connection to Particle Formation. *Tellus, Ser. B* **2008**, *60* (4), 495−508.

DOI: 10.1021/acs.est.9b05306
Environ. Sci. Technol. 2019, 53, 14387−14397

(75) Jayaratne, R.; Pushpawela, B.; He, C. R.; Li, H.; Gao, J.; Chai, F. H.; Morawska, L. Observations of Particles at Their Formation Sizes in Beijing, China. *Atmos. Chem. Phys.* **2017**, *17* (14), 8825−8835.
(76) Qi, X. M.; Ding, A. J.; Nie, W.; Petaja, T.; Kerminen, V. M.; Herrmann, E.; Xie, Y. N.; Zheng, L. F.; Manninen, H.; Aalto, P.; Sun, J. N.; Xu, Z. N.; Chi, X. G.; Huang, X.; Boy, M.; Virkkula, A.; Yang, X. Q.; Fu, C. B.; Kulmala, M. Aerosol Size Distribution and New Particle Formation in the Western Yangtze River Delta of China: 2 Years of Measurements at the SORPES Station. *Atmos. Chem. Phys.* **2015**, *15* (21), 12445−12464.
(77) Elm, J. An Atmospheric Cluster Database Consisting of Sulfuric Acid, Bases, Organics, and Water. *ACS Omega* **2019**, *4* (6), 10965−10974.
(78) Schobesberger, S.; Junninen, H.; Bianchi, F.; Lonn, G.; Ehn, M.; Lehtipalo, K.; Dommen, J.; Ehrhart, S.; Ortega, I. K.; Franchin, A.; Nieminen, T.; Riccobono, F.; Hutterli, M.; Duplissy, J.; Almeida, J.; Amorim, A.; Breitenlechner, M.; Downard, A. J.; Dunne, E. M.; Flagan, R. C.; Kajos, M.; Keskinen, H.; Kirkby, J.; Kupc, A.; Kurten, A.; Kurtén, T.; Laaksonen, A.; Mathot, S.; Onnela, A.; Praplan, A. P.; Rondo, L.; Santos, F. D.; Schallhart, S.; Schnitzhofer, R.; Sipila, M.; Tome, A.; Tsagkogeorgas, G.; Vehkamäki, H.; Wimmer, D.; Baltensperger, U.; Carslaw, K. S.; Curtius, J.; Hansel, A.; Petaja, T.; Kulmala, M.; Donahue, N. M.; Worsnop, D. R. Molecular understanding of atmospheric particle formation from sulfuric acid and large oxidized organic molecules. *Proc. Natl. Acad. Sci. U. S. A.* **2013**, *110* (43), 17223−17228.
(79) Liu, L.; Kupiainen-Maatta, O.; Zhang, H.; Li, H.; Zhong, J.; Kurtén, T.; Vehkamäki, H.; Zhang, S.; Zhang, Y.; Ge, M.; Zhang, X.; Li, Z. Clustering Mechanism of Oxocarboxylic Acids Involving Hydration Reaction: Implications for the Atmospheric Models. *J. Chem. Phys.* **2018**, *148* (21), 214303.
(80) Henschel, H.; Kurtén, T.; Vehkamäki, H. Computational Study on the Effect of Hydration on New Particle Formation in the Sulfuric Acid/Ammonia and Sulfuric Acid/Dimethylamine Systems. *J. Phys. Chem. A* **2016**, *120* (11), 1886−1896.
(81) DePalma, J. W.; Doren, D. J.; Johnston, M. V. Formation and Growth of Molecular Clusters Containing Sulfuric Acid, Water, Ammonia, and Dimethylamine. *J. Phys. Chem. A* **2014**, *118* (29), 5464−5473.
(82) Kurtén, T.; Kuang, C. A.; Gomez, P.; McMurry, P. H.; Vehkamäki, H.; Ortega, I.; Noppel, M.; Kulmala, M. The Role of Cluster Energy Nonaccommodation in Atmospheric Sulfuric Acid Nucleation. *J. Chem. Phys.* **2010**, *132*, 024304.
(83) Lin, Y.; Ji, Y. M.; Li, Y. X.; Secrest, J.; Xu, W.; Xu, F.; Wang, Y.; An, T. C.; Zhang, R. Y. Interaction between Succinic Acid and Sulfuric Acid-base Clusters. *Atmos. Chem. Phys.* **2019**, *19* (12), 8003−8019.
(84) Lee, S. H.; Gordon, H.; Yu, H.; Lehtipalo, K.; Haley, R.; Li, Y. X.; Zhang, R. Y. New Particle Formation in the Atmosphere: From Molecular Clusters to Global Climate. *J. Geophys. Res.-Atmos.* **2019**, *124* (13), 7098−7146.
(85) Maergoiz, A. I.; Nikitin, E. E.; Troe, J.; Ushakov, V. G. Classical Trajectory and Adiabatic Channel Study of the Transition from Adiabatic to Sudden Capture Dynamics. III. Dipole-dipole Capture. *J. Chem. Phys.* **1996**, *105* (15), 6277−6284.
(86) Georgievskii, Y.; Klippenstein, S. J. Long-range Transition State Theory. *J. Chem. Phys.* **2005**, *122*, 194103.
(87) Duporte, G.; Riva, M.; Parshintsev, J.; Heikkinen, E.; Barreira, L. M. F.; Myllys, N.; Heikkinen, L.; Hartonen, K.; Kulmala, M.; Ehn, M.; Riekkola, M. L. Chemical Characterization of Gas- and Particle-Phase Products from the Ozonolysis of alpha-Pinene in the Presence of Dimethylamine. *Environ. Sci. Technol.* **2017**, *51* (10), 5602−5610.
(88) Duporte, G.; Parshintsev, J.; Barreira, L. M.; Hartonen, K.; Kulmala, M.; Riekkola, M. L. Nitrogen-Containing Low Volatile Compounds from Pinonaldehyde-Dimethylamine Reaction in the Atmosphere: A Laboratory and Field Study. *Environ. Sci. Technol.* **2016**, *50* (9), 4693−700.

DOI: 10.1021/acs.est.9b05306
Environ. Sci. Technol. 2019, 53, 14387−14397